

# Tunnel junction thermometry down to millikelvin temperatures

A. V. Feshchenko,<sup>1,\*</sup> L. Casparis,<sup>2,†</sup> I. M. Khaymovich,<sup>1</sup> D. Maradan,<sup>2</sup> O.-P. Saira,<sup>1</sup> M. Palma,<sup>2</sup> M. Meschke,<sup>1</sup> J. P. Pekola,<sup>1</sup> and D. M. Zumbühl<sup>2</sup>

<sup>1</sup>*Low Temperature Laboratory, Department of Applied Physics,  
Aalto University, P. O. Box 13500, FI-00076 AALTO, Finland*

<sup>2</sup>*Department of Physics, University of Basel, CH-4056 Basel, Switzerland*

(Dated: December 7, 2024)

We present a simple on-chip electronic thermometer with the potential to operate down to 1 mK. It is based on transport through a single normal metal - superconductor tunnel junction with rapidly widening leads. The current through the junction is determined by the temperature of the normal electrode that is efficiently thermalized to the phonon bath, and it is virtually insensitive to the temperature of the superconductor, even when the latter is relatively far from equilibrium. We demonstrate here operation of the device down to 7 mK. A systematic thermal analysis shows that temperatures down to 1 mK are within reach.

On-chip electronic thermometry is an important part of modern research and commercial applications of nanotechnology and it has been studied already for several decades, see [1] and references therein. Many of these thermometers are based on tunnel junctions or quantum dots [2–4]. Temperature sensors based on normal (N) and superconducting (S) metal tunnel junctions are used in a wide range of experiments [5–7] and applications [8, 9]. An example of such a device is a primary Coulomb blockade thermometer (CBT) that is based on normal metal tunnel junctions with an insulator ‘I’ as a tunnel barrier (NIN) [10, 11], where the electronic temperature can be obtained by measuring the full width at half minimum of the conductance dip,  $V_{1/2}$ . One more example is an SNS thermometer [12], whose critical current  $I_c$  depends strongly on temperature. Primary electronic thermometry has also been successfully demonstrated down to 10 mK using shot noise of a tunnel junction (SNT) [13–15]. Nevertheless, a thermometer that has a modest structure and a simple but accurate temperature reading at sub-10 mK temperatures, and does not require a complicated experimental setup is still missing. For this purpose we present an NIS junction that is widely used both as a refrigerating element and a probe of the local electronic temperature in different experiments and applications [5–9, 16–18]. The possibility to use the NIS junction at sub-10 mK temperatures makes this thermometer suited for cryogenic applications at low temperatures, for example, as a thermometer for a dilution refrigerator. The low temperature scientific community can also benefit from this sensor for research purposes, since the NIS thermometer can be combined on-chip with other solid state devices. The NIS thermometer is easy to operate compared to SNT [13, 14] and its thermalization is quite straightforward compared to CBT [11] due to the single junction configuration. A measurement of the NIS current-voltage ( $I - V$ ) characteristic yields a primary temperature reading.

In this Article, we study both experimentally and theoretically an on-chip electronic thermometer based on a

single NIS tunnel junction at sub-10 mK temperatures. For the first time, we demonstrate the operation of the NIS thermometer down to 7.3 mK. In addition, we develop a thermal model that explains our measurement data and further shows that selfheating effects remain negligible for temperatures down to 1 mK.

Transport through an NIS junction has strong bias and temperature dependence. Near zero bias voltage the current is suppressed due to the superconducting gap,  $\Delta$  [19]. When biased at voltage  $V$ , current depends on temperature due to the broadening of the Fermi distribution  $f_N(E) = (e^{E/k_B T_N} + 1)^{-1}$  in the normal metal with the temperature  $T_N$  and the Boltzmann constant  $k_B$ . The current can be expressed as [19]

$$I = \frac{1}{2eR_T} \int dE n_s(E) [f_N(E - eV) - f_N(E + eV)], \quad (1)$$

where  $R_T$  is the tunneling resistance of the junction.

In the superconductor, the Bardeen-Cooper-Schrieffer (BCS) density of states (DOS) is smeared and typically described by the Dynes parameter  $\gamma$  expressed as  $n_s(E) = |\Re e(u/\sqrt{u^2 - 1})|$ , where  $u = E/\Delta(T_S) + i\gamma$  and  $T_S$  is the temperature of the superconductor. Possible origins of  $\gamma$  include broadening of the quasiparticle energy levels due to finite life time [20], Andreev current [21, 22], as well as photon assisted tunneling caused by high-frequency noise and black-body radiation [23]. The typical experimental range of  $\gamma$  is  $10^{-4}$  to  $10^{-5}$  for a single NIS junction [23], getting as low as  $10^{-7}$  in SI-NIS single electron transistors with multistage shielding [24, 25].

One can determine  $T_N$  from a measured  $I - V$  curve using Eq. (1). As we show below, the selfheating of both N and S electrodes has a small effect on the  $I - V$  characteristic, thus for now we neglect these effects. Therefore, we assume temperatures to be small,  $k_B T_{N,S} \ll eV, \Delta(T_S)$ , and the superconducting gap to be constant and equal to its zero-temperature value  $\Delta$ . In this case for  $eV < \Delta$ ,

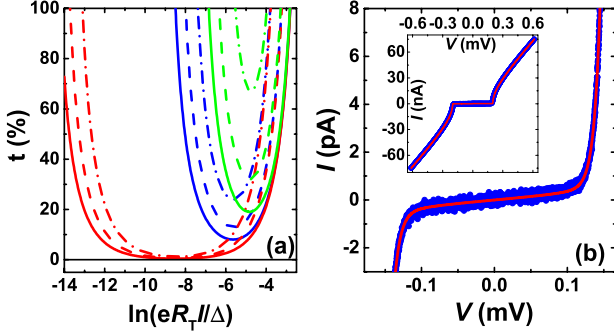


FIG. 1. (Color online) In panel (a), we show the relative deviation of the present thermometer reading using method *B* with a numerically calculated  $I - V$ , Eq. (1). Sets of curves present the values of  $t$  for three  $\gamma$  parameters:  $10^{-7}$ ,  $2.2 \times 10^{-5}$  (the actual value in the experiment),  $10^{-4}$  and shown as red, blue and green curves from left to right. For each  $\gamma$  parameter temperatures 1, 3, and 7 mK are shown as dash-dotted, dashed and solid lines, respectively. All curves are calculated using the parameters of the measured device with  $\Delta = 200$   $\mu\text{eV}$  and  $R_T = 7.7$   $\text{k}\Omega$ . The main panel (b), shows the measured  $I - V$  characteristic (blue dots) together with full fit (solid red line) zoomed in the superconducting gap region. (Inset) Measured and calculated  $I - V$  curve on a wider voltage scale at  $\sim 10$  mK.

one can approximate Eq. (1) by

$$I \simeq I_0 e^{-(\Delta - eV)/k_B T_N} + \frac{\gamma V}{R_T \sqrt{1 - (eV/\Delta)^2}}, \quad (2)$$

where  $I_0 = \sqrt{2\pi\Delta k_B T_N}/2eR_T$  [6, 21]. Here the second term stands for the corrections to the  $I - V$  characteristic due to smearing. It leads to the saturation of the exponential increase of the current at low bias values. In the regime of moderate bias voltages, one can neglect this term and invert Eq. (2) into

$$V = \frac{\Delta}{e} + \frac{k_B T_N}{e} \ln(I/I_0). \quad (3)$$

This equation provides a way to obtain the electronic temperature  $T_N^B$  only by the fundamental constants and by the slope of the measured  $I - V$  characteristic on a semilogarithmic scale as

$$T_N^B(V) = \frac{e}{k_B} \frac{dV}{d(\ln I)}. \quad (4)$$

This allows us to use NIS junction as a primary thermometer, however, with some limitations. One can include the effects of  $\gamma$  into Eq. (4) by subtracting the last term in Eq. (2) from the current  $I$  and obtain a better accuracy. We do not take this approach here, since the main advantage of Eq. (4) is its simplicity as a primary thermometer without any fitting parameters.

Next, we will compare the two methods used to extract the electronic temperature from the measured  $I - V$

curves. In method *A*, we employ Eq. (1) and perform a non-linear least-squares fit of a full  $I - V$  characteristic with  $T_N$  as the only free parameter. The value of  $T_N$  obtained in this manner, named  $T_N^A$ , is not sensitive to  $\gamma$ . Method *B* is based on the local slope of the  $I - V$  (see Eq. (4)). The smearing parameter  $\gamma$  has an influence on the slope of the  $I - V$  characteristic and thus induces errors in the temperature determination. The temperature  $T_N^B$  is extracted as the slope of measured  $\ln I$  vs  $V$  over a fixed  $I$  range for all temperatures where Eq. (4) is valid. In the experiment it is usually difficult to determine the environment parameters precisely, but one can determine  $\gamma$  from the ratio of  $R_T$  and the measured zero bias resistance of the junction. The  $I - V$  which takes the  $\gamma$  parameter into account (see Eq. (2)) gives indistinguishable results from the ones obtained by method *A*.

We evaluate the influence of the  $\gamma$  parameter on the relative deviations of the present thermometer based on method *B* numerically, as shown in Fig. 1 (a). This deviation,  $t$ , is defined as the relative error  $t = (T_N^B/T_N) - 1$ . We show the values of  $t$  vs  $\ln(eR_T I/\Delta)$  for two extreme cases  $\gamma = 10^{-7}$ ,  $10^{-4}$  and for  $\gamma = 2.2 \times 10^{-5}$  extracted from the present experiment at temperatures of 1, 3 and 7 mK. The lowest bath temperature is 3 mK and 7 mK is the saturation of the electronic temperature in the current experiment. The larger the values of  $\gamma$  and the lower the temperature, the higher the relative deviations. In addition, the range of the slope used to extract  $T_N^B$  shrinks with increasing  $\gamma$  and with decreasing temperature (see e.g. red curves, Fig. 1 (a)). Thus reducing the leakage will significantly improve the accuracy of the device, especially towards lower temperatures. Possible avenues for suppressing  $\gamma$  include improved shielding [24, 26] and encapsulating the device between ground planes, intended to reduce the influence of the electromagnetic environment [23]. Finally, higher tunneling resistance of the junction decreases Andreev current [27]. We note that one can also use  $dV/d(\ln g)$  as a primary thermometer, where  $g = dI/dV$  is the differential conductance - typically a more precise measurement since it is done with a lock-in technique. Compared to Eq. (4) this reduces the minimal deviation  $t$  by at least a factor of 3.5 for  $T_N \geq 1$  mK (6 for  $T_N \geq 10$  mK), though exhibiting qualitatively similar dependencies on  $\gamma$  and  $T_N$ .

Next, we describe the realization of the NIS thermometer that is shown together with a schematic of the experimental setup in the scanning-electron micrograph (SEM) in Fig. 2. The device is made by electron beam lithography and two-angle shadow evaporation technique [28]. The ground plane under the junction is made out of 50 nm of Au. To electrically isolate the ground plane from the junction, we cover the Au layer with 100 nm of  $\text{AlO}_x$  using atomic layer deposition. Next, we deposit a layer of  $d_S = 40$  nm of Al that is thermally oxidized *in situ*. The last layer is formed immediately after the oxidation pro-

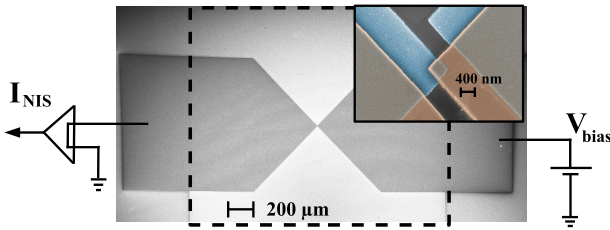


FIG. 2. (Color online) A scanning-electron micrograph of the NIS device together with a schematic of the experimental setup. In the main panel S and N leads of the junction are visible, underneath the pads the ground plane of a square shape is indicated by a dashed line. Zoom into the actual tunnel junction (see inset), where S and N layers are colored in blue and brown, respectively.

cess by deposition of  $d_N = 150$  nm of Cu, thus creating an NIS tunnel junction with an area  $A = 380$  nm  $\times$  400 nm. The geometry of the junction is chosen such that the leads immediately open up at an angle of 90° and create large pads with an area  $A_N = A_S = 1.25$  mm $^2$  providing good thermalization. The S lead is covered by a thick normal metal shadow as shown in the inset of Fig. 2 by brown color, where N and S layers are interfaced by the same insulating layer of AlO<sub>x</sub> as the junction.

The experiment is performed in a dilution refrigerator (base temperature 9 mK) where each of the sample wires is cooled by its own, separate Cu nuclear refrigerator [29], here providing bath temperatures  $T_{bath}$  down to 3 mK. Nuclear refrigerator temperatures after demagnetization are highly reproducible and obtained from the precooling temperatures and previously determined efficiencies [11]. Temperatures above  $\sim 9$  mK are measured with a cerium magnesium nitrate thermometer which was calibrated against a standard superconducting fixed point device. Since the sample is sensitive to magnetic fields, compensation of the demagnetization field to below 1 G is done using the sample magnet. The I-V curves (see Fig. 2 for the electrical circuit) are measured using a home-built current preamplifier with input offset-voltage stabilization [30] to minimize distortions in the I-V curves.

Filtering, radiation shielding and thermalization is crucial for obtaining a low  $\gamma$  and low device temperatures. Each sample wire is going through 1.6 m of thermocoax, followed by a silver epoxy microwave filter [31], a 30 kHz low-pass filter and a sintered silver heat exchanger in the mixing chamber before passing the Al heat switch and entering the Cu nuclear stage. The setup is described in detail in Ref. 11 and has been further improved here. First, the ceramic chip carrier was replaced by silver epoxy parts which remain metallic to the lowest temperatures, allowing more efficient cooling. Further, the sample – previously mounted openly inside the cold-plate radiation shield together with the nuclear stages – is enclosed in an additional silver shield, sealed with silver paint against the silver epoxy socket and thermalized to

one of the Cu refrigerators. Finally, each wire is fed into the sample shield through an additional silver epoxy microwave filter. While previously saturating at 10 mK or above [11], metallic CBTs have given temperatures around 7 mK after the improvements [31], comparable to the NIS temperatures presented here.

In Fig. 1 (b), the measured  $I$ - $V$  characteristic in the superconducting gap region is shown by blue dots. The solid red line corresponds to the full fit based on method A. In the inset, we present the  $I$ - $V$  characteristic at larger voltage scale, used to extract  $R_T$ . In Fig. 3 (a),

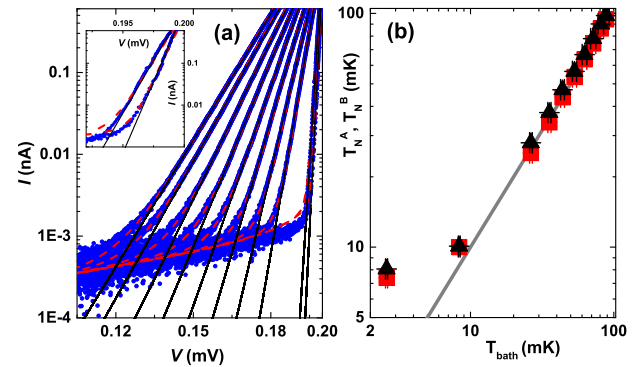


FIG. 3. (Color online) Panel (a) shows measured  $I$ - $V$ 's (blue dots), when  $T_{bath}$  is lowered from left to right together with fits as solid black and dashed red lines (see text). (Inset) close-up of two  $I$ - $V$ 's for temperatures of 10 and 7 mK. The electronic temperature extracted from both the full fit (red squares) of the  $I$ - $V$ 's and its slope (black points) are shown in (b).

the measured  $I$ - $V$ 's of the NIS junction are shown in logarithmic scale by blue dots at  $T_{bath} = 100 \dots 3$  mK from left to right. The full fits are shown as dashed red lines. The tunneling resistance  $R_T = 7.7$  k $\Omega$  and the Dynes parameter  $\gamma = 2.2 \times 10^{-5}$ , used in all these fits were determined based on the  $I$ - $V$ 's shown in Fig. 1 (b) at high and low voltages, respectively. The superconducting gap cannot be accurately determined independently of  $T_N$ , moreover at the lowest  $T_N$  the sensitivity to the gap is large. However, Eq. (1) gives a possibility to perform a non-linear least-squares fit and Eq. (3) gives a linear fit, where the parameters  $\Delta$  and  $T_N$  are responsible for the offset and the slope, respectively. Therefore at high temperatures, one can narrow the range of  $\Delta$  values so much that  $T_N$  becomes essentially an independent parameter for the fits. Thus the gap extracted from the high temperature data using Eq. (1) remains fixed,  $\Delta = 200 \pm 0.5$   $\mu$ eV, for all the lower temperatures. In addition, we show as solid black lines an exponential  $I$  –  $V$  dependence corresponding to method B with a fitting range between 5 pA and 400 pA. The inset shows zoom of the  $I$  –  $V$  curves at temperatures of 10 and 7 mK. The  $I$ - $V$  characteristics presented in Fig. 3 (a) agree well with the theoretical expressions in Eqs. (1) and (2) (the latter form is not

shown). In Fig. 3 (b), we show the electronic temperatures obtained using method *A* (red squares) and method *B* (black triangles) vs  $T_{bath}$ . Method *A* (*B*) shows a relative error in the electronic temperature up to 6 % (11 %). The error in method *B* is larger, as we neglect the influence of the  $\gamma$  parameter.

The lowest temperature obtained from the full fit is  $T_N^A = 7.3$  mK with statistical uncertainty of 5 % at  $T_{bath} = 3$  mK. The NIS temperature decreases slowly over time, arriving at 7.3 mK several weeks after the cool down from room temperature. This suggests that internal relaxation causing a time-dependent heat leak e.g. in the silver epoxy sample holder is limiting the minimum temperature. Future improvements will employ low heat-release materials better suited for ultra-low temperatures such as sapphire or pure, annealed metals e.g. for the socket and chip carrier, minimizing organic, noncrystalline substances such as epoxies.

So far we neglected all selfheating effects both in the normal metal and in the superconductor. To justify this no-selfheating assumption, we numerically and analytically check the selfheating effects both in the normal metal and in the superconductor. We sketch the analytical arguments below. The total power dissipated in the device is equal to  $IV = \dot{Q}_{NIS}^N + \dot{Q}_{NIS}^S$ , where  $\dot{Q}_{NIS}^N$  and  $\dot{Q}_{NIS}^S$  are the heat powers to the normal metal and to the superconductor, respectively. The heat released to the superconductor is given by

$$\dot{Q}_{NIS}^S = \frac{1}{e^2 R_T} \int E_S n_s(E) [f_N(E - eV) - f_S(E)] dE, \quad (5)$$

where  $E_S = E$  is the quasiparticle energy. To evaluate  $\dot{Q}_{NIS}^S$  one has to substitute  $E_S$  by  $E_N = (eV - E)$  in Eq. (5). Almost all of the heat is delivered to the superconductor in the measured (subgap) bias range, thus  $\dot{Q}_{NIS}^S \sim IV$  and  $\dot{Q}_{NIS}^N \ll \dot{Q}_{NIS}^S$ .

First, we consider the selfheating of the superconductor. It can occur due to the exponential suppression of thermal conductivity and the weak electron-phonon (e-ph) coupling, especially at low temperatures. We study the heat transport in the present geometry (see Fig. 2) by a diffusion equation

$$-\nabla(\kappa_S \nabla T_S) = u_S, \quad (6)$$

where we set a boundary condition near the junction  $-\bar{n}_{inner} \kappa_S \nabla T_S|_{junct} = \dot{Q}_{NIS}^S / A$ , where  $\bar{n}_{inner}$  is the inner normal to the junction. Thermal conductivity in the superconductor is  $\kappa_S = \frac{6}{\pi^2} \left( \frac{\Delta}{k_B T_S} \right)^2 e^{\frac{-\Delta}{k_B T_S}} L_0 T_S \sigma_{Al}$ , where  $L_0$  is the Lorenz number and  $\sigma_{Al} = 3 \times 10^7$  ( $\Omega m$ ) $^{-1}$  is the electrical conductivity of the Al film in the normal state [32], and we take into account the  $T_S$  dependence of the gap at low temperatures,  $\Delta(T_S)/\Delta(0) \simeq 1 - \sqrt{2\pi k_B T_S/\Delta} e^{-\Delta/k_B T_S}$ . The absorbed heat is given by  $u_S = \dot{q}_{e-ph,S}^S + \dot{q}_{trap}$ . Here, the first term is the electron-phonon power  $\dot{q}_{e-ph,S}^S \simeq \Sigma_{Al} (T_S^5 - T_p^5) \exp(-\Delta/k_B T_S)$

[33], where  $\Sigma_{Al} = 3 \times 10^8$   $WK^{-5}m^{-3}$  is the material dependent electron-phonon coupling constant. The phonon temperature,  $T_p$ , is assumed to be equal to  $T_{bath}$ . Due to weak electron-phonon coupling nearly all the heat is released through the (unbiased) normal metal shadow (see Fig. 4) that acts as a trap for quasiparticles,  $\dot{q}_{trap}$ . Here

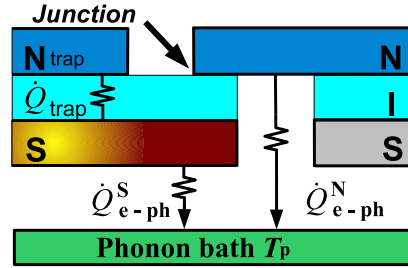


FIG. 4. (Color online) The thermal diagram of the NIS thermometer. Present schematic does not reflect the real thicknesses of the materials. In this thermal model we assume the normal metal shadow that acts as the trap to be at  $T_{bath}$ .

the conductance of the trap per unit area is the same as for the tunnel junction  $\sigma_T = 1/(R_T A)$ . Therefore, the heat removed per volume by this trap  $\dot{q}_{trap}$  can be calculated using Eq. (5) at  $V = 0$ ,  $T_N = T_{bath}$  and substituting  $R_T$  by  $d_S/\sigma_T$ . Thus the temperature of the superconductor,  $T_S$ , can be found as the solution of Eq. (6) and can be written as [32]  $\sqrt{2\pi k_B T_S/\Delta(T_S)} e^{-\Delta(T_S)/k_B T_S} \equiv \alpha \dot{Q}_{NIS}^S$ . Here we indeed assume  $\dot{Q}_{NIS}^S \sim IV$ , and  $\alpha = \sqrt{\pi} e^2 G / (d_S \sigma_{Al} \sqrt{2k_B T_S \Delta^3(T_S)})$  is a coefficient that depends on  $T_S$  and dimensionless parameter  $G \sim 2 \dots 3$  is logarithmically dependent on the sample geometry [32]. After substitution of all the parameters, we find that the superconductor temperature  $T_S$  stays below 250 mK in bias range  $|V| \leq \frac{\Delta}{e}$ , and does not influence the thermometer reading. In this bias range and at  $T_{bath} = 3$  mK, from the numerical calculations we estimate the temperature of the superconductor  $T_S = 145$  mK and the power injected to the superconductor is  $IV \sim 90$  fW. At the same time we evaluate the relative change of the slope to be small  $|t| \lesssim 5 \times 10^{-3}$  at  $I \lesssim 1$  nA. As a conclusion, the temperatures obtained from both methods *A* and *B* are affected by less than 0.5 % by selfheating of the superconductor.

Selfheating of the normal metal that might occur due to weak electron-phonon coupling and back flow of heat from the superconductor [34]. One can solve the diffusion equation Eq. (6) with the same boundary condition as above by replacing all S indices by N, where  $\kappa_N = L_0 \sigma_{Cu} T_N$  is the thermal conductivity of the normal metal, and the electrical conductivity of Cu is assumed to be  $\sigma_{Cu} = 5 \times 10^7$  ( $\Omega m$ ) $^{-1}$  [35]. The heat absorbed in the normal metal is  $u_N = \dot{q}_{e-ph,N}^N + \dot{q}_{wire}^N$ . The heat conduction through the gold bonding wires,  $\dot{q}_{wire}^N$ , is taken into account only at the point, where it is attached to the normal metal pad, whereas the electron-

phonon interaction  $\dot{q}_{e-ph}^N$  is effective in the full volume of the normal metal. The volumetric electron-phonon power is  $\dot{q}_{e-ph}^N = \Sigma_{Cu}(T_N^5 - T_p^5)$ , where  $\Sigma_{Cu} = 2 \times 10^9 \text{ W K}^{-5} \text{ m}^{-3}$  is the electron-phonon coupling constant of copper. Here we consider the effect of the heat removed by the bonding wires on the temperature only in the normal metal, thus  $\dot{q}_{wire}^N = L_0 \sigma_{Au}(T_N^2 - T_{bath}^2)/2L_{wire}d_N$ . The length of the gold bonding wire is  $L_{wire} = 5 \text{ mm}$  and  $\sigma_{Au} = 1.8 \times 10^9 \text{ (\Omega m)}^{-1}$  is the electrical conductivity of gold, measured at low temperatures. The thermal relaxation length in the normal metal [1] is  $l_N = (T_{bath}^{p/2-1})^{-1} \sqrt{(\sigma_{Cu} L_0 / (2\Sigma_{Cu}))}$ . We substitute  $p = 5$  and  $T_{bath} = 10 \text{ mK}$ , and obtain  $l_N = 17.5 \text{ mm}$ . Since all the dimensions of the present device are smaller than 1.5 mm, there is only a weak temperature gradient over the normal metal electrode due to its good heat conduction, and the electron-phonon coupling weakened at low temperatures. By solving the heat balance equation  $\dot{Q}_{NIS}^N = \dot{Q}_{e-ph}^N + \dot{Q}_{wire}^N$  and assuming no external heat leaks, one can calculate  $T_N$ . Here, the heat released through e-ph coupling is  $\dot{Q}_{e-ph}^N = \Omega_N \dot{q}_{e-ph}^N$ , where  $\Omega_N = A_N d_N$  is the volume of the N electrode. The heat released through  $N_{wire} = 2$  bonding wires is  $\dot{Q}_{wire}^N = \dot{q}_{wire}^N N_{wire} A_{wire} d_N$ , where its cross sectional area is  $A_{wire} = \pi r_{wire}^2$  with a radius  $r_{wire} = 16 \mu\text{m}$ . The temperature obtained from both methods A and B are affected by less than 0.5 % by selfheating of the normal metal down to 1 mK temperature. In addition, we can evaluate at low temperatures  $T_N \leq T_S \ll \Delta / k_B$  the maximum cooling at optimum bias voltage [1] to be 90 pW at  $T_{bath} = 1 \text{ mK}$ .

In conclusion, we have demonstrated experimentally the operation of an electronic thermometer based on a single NIS tunnel junction. The thermometer agrees well with the refrigerator thermometer down to about 10 mK and reaches a lowest temperature of 7.3 mK at  $T_{bath} = 3 \text{ mK}$ , currently limited by a time-dependent heat leak to the sample stage. We have discussed several possible improvements of the present device and experimental setup. Finally, we have shown that selfheating in the normal metal and in the superconductor on the full  $I$ - $V$  or its slope is negligible, paving the way for NIS thermometry down to 1 mK if the experimental challenges can be overcome.

We would like to thank G. Frossati, G. Pickett, V. Shvarts, and M. Steinacher for valuable inputs. We acknowledge the availability of the facilities and technical support by Otaniemi research infrastructure for Micro and Nanotechnologies (OtaNano). We acknowledge financial support from the European Community FP7 Marie Curie Initial Training Networks Action (ITN) Q-NET 264034, MICROKELVIN (project no. 228464), SOLID, INFERNOS (project no. 308850), EMRP (project no. SIB01-REG2) and the Academy of Finland though its LTQ CoE grant (project no. 250280). This work was supported by Swiss Nanoscience Insti-

tute (SNI), NCCR QSIT, Swiss NSF, and ERC starting grant.

\* anna.feshchenko@aalto.fi; Contributed equally to this work

† Contributed equally to this work

- [1] F. Giazotto, T. T. Heikkilä, A. Luukanen, A. M. Savin, and J. P. Pekola, Rev. Mod. Phys. **78**, 217 (2006).
- [2] S. Gasparinetti, F. Deon, G. Biasiol, L. Sorba, F. Beltram, and F. Giazotto, Phys. Rev. B **83**, 201306 (2011).
- [3] A. Mavalankar, S. J. Chorley, J. Griffiths, G. A. C. Jones, I. Farrer, D. A. Ritchie, and C. G. Smith, Appl. Phys. Lett. **103**, 133116 (2013).
- [4] D. Maradan, L. Casparis, T.-M. Liu, D. Biesinger, C. Scheller, D. Zumbühl, J. Zimmerman, and A. Gossard, J. Low Temp. Phys. **175**, 784 (2014).
- [5] M. Nahum and J. M. Martinis, Appl. Phys. Lett. **63**, 3075 (1993).
- [6] M. Nahum, T. M. Eiles, and J. M. Martinis, Appl. Phys. Lett. **65**, 3123 (1994).
- [7] A. V. Feshchenko, J. V. Koski, and J. P. Pekola, Phys. Rev. B **90**, 201407(R) (2014).
- [8] A. M. Clark, A. Williams, S. T. Ruggiero, M. L. van den Berg, and J. N. Ullom, Appl. Phys. Lett. **84**, 625 (2004).
- [9] N. A. Miller, G. C. O'Neil, J. A. Beall, G. C. Hilton, K. D. Irwin, D. R. Schmidt, L. R. Vale, and J. N. Ullom, Appl. Phys. Lett. **92**, 163501 (2008).
- [10] J. P. Pekola, K. P. Hirvi, J. P. Kauppinen, and M. A. Paalanen, Phys. Rev. Lett. **73**, 2903 (1994).
- [11] L. Casparis, M. Meschke, D. Maradan, A. C. Clark, C. P. Scheller, K. K. Schwarzwälder, J. P. Pekola, and D. M. Zumbühl, Rev. Sci. Instrum. **83**, 083903 (2012).
- [12] P. Dubos, H. Courtois, B. Pannetier, F. K. Wilhelm, A. D. Zaikin, and G. Schön, Phys. Rev. B **63**, 064502 (2001).
- [13] L. Spietz, K. W. Lehnert, I. Siddiqi, and R. J. Schoelkopf, Science **300**, 1929 (2003).
- [14] L. Spietz, R. J. Schoelkopf, and P. Pari, Appl. Phys. Lett. **89**, 183123 (2006).
- [15] L. F. Spietz, *The Shot Noise Thermometer*, Ph.D. thesis (2006).
- [16] M. M. Leivo, J. P. Pekola, and D. V. Averin, Appl. Phys. Lett. **68**, 1996 (1996).
- [17] P. A. Fisher, J. N. Ullom, and M. Nahum, Appl. Phys. Lett. **74**, 2705 (1999).
- [18] J. T. Muhonen, M. Meschke, and J. P. Pekola, Rep. Prog. Phys. **75**, 046501 (2012).
- [19] M. Tinkham, *Introduction to superconductivity*, 2nd ed. (Dover, New York, 1996).
- [20] R. C. Dynes, V. Narayanamurti, and J. P. Gorno, Phys. Rev. Lett. **41**, 1509 (1978).
- [21] H. Courtois, S. Rajauria, P. Gandit, F. Hekking, and B. Pannetier, J. Low Temp. Phys. **153**, 325 (2008).
- [22] T. Greibe, M. P. V. Stenberg, C. M. Wilson, T. Bauch, V. S. Shumeiko, and P. Delsing, Phys. Rev. Lett. **106**, 097001 (2011).
- [23] J. P. Pekola, V. F. Maisi, S. Kafanov, N. Chekurov, A. Kemppinen, Y. A. Pashkin, O.-P. Saira, M. Möttönen, and J. S. Tsai, Phys. Rev. Lett. **105**, 026803 (2010).
- [24] O.-P. Saira, A. Kemppinen, V. F. Maisi, and J. P.

Pekola, Phys. Rev. B **85**, 012504 (2012).

[25] H. Q. Nguyen, M. Meschke, H. Courtois, and J. P. Pekola, Phys. Rev. Appl. **2**, 054001 (2014).

[26] J. M. Hergenrother, J. G. Lu, M. T. Tuominen, D. C. Ralph, and M. Tinkham, Phys. Rev. B **51**, 9407 (1995).

[27] F. W. J. Hekking and Y. V. Nazarov, Phys. Rev. B **49**, 6847 (1994).

[28] T. A. Fulton and G. J. Dolan, Phys. Rev. Lett. **59**, 109 (1987).

[29] A. C. Clark, K. K. Schwarzländer, T. Bandi, D. Maradan, and D. M. Zumbühl, Rev. Sci. Instrum. **81**, 103904 (2010).

[30] Low noise/high stability I to V converter SP893, M. Steinacher, Electronics lab, Physics, University of Basel.

[31] C. P. Scheller, S. Heizmann, K. Bedner, D. Giss, M. Meschke, D. M. Zumbühl, J. D. Zimmerman, and A. C. Gossard, Appl. Phys. Lett. **104**, 211106 (2014).

[32] H. S. Knowles, V. F. Maisi, and J. P. Pekola, Appl. Phys. Lett. **100**, 262601 (2012).

[33] A. V. Timofeev, C. P. Garcia, N. B. Kopnin, A. M. Savin, M. Meschke, F. Giazotto, and J. P. Pekola, Phys. Rev. Lett. **102**, 017003 (2009).

[34] J. Jochum, C. Mears, S. Golwala, B. Sadoulet, J. P. Castle, M. F. Cunningham, O. B. Drury, M. Frank, S. E. Labov, F. P. Lipschultz, H. Netel, and B. Neuhauser, J. Appl. Phys. **83**, 3217 (1998).

[35] J. Pekola, A. Manninen, M. Leivo, K. Arutyunov, J. Suoknuuti, T. Suppula, and B. Collaudin, Physica B: Condensed Matter **280**, 485 (2000).